Trans. JWRI, Vol. 25(1996), No.2

Analytical Approach to Anode Boundary Layer of Gas Tungsten Arcs

by Masao USHIO, Manabu TANAKA and Chuan Song WU

Joining and Welding Research Institute, Osaka University
Ibaraki, Osaka, Japan

Abstract

In order to make clear the heat transfer phenomena at the anode boundary layer of gas-tungsten-arcs, the plasma properties were measured by using laser scattering method and Langmuir probe method. Experiments revealed that physical properties were strongly influenced by the arc current. In case of low current (50 A), anode boundary layer was ~250 mm in thickness in which electron temperature was considerably different with that of heavy particle temperature and the space potential in the boundary layer was low with respect to the anode. With increasing in arc current, however, the thickness of boundary layer became narrow and the space potential in the layer changed to higher value with respect to the anode in the case of 150 A in arc current.

Numerical analysis of anode region was carried out to understand above experimental results. The anode region was divided into three subzones: the anode boundary layer, the presheath and the sheath. The governing equations of the dominating processes with the boundary conditions taken from the solutions of LTE plasmas, were solved by applying the Runge-Kutta procedure. Two parameters θ and α were introduced into this study. The former is the ratio of the heavy particle temperature at the free-fall edge to the anode surface temperature while the latter is the percentage of the electrons entering the lattice of anode. The results indicated that the parameter θ was an important factor influencing the local plasma properties in the boundary layer, the boundary layer thickness and the sheath potential. An estimate of the potential drop in the boundary layer showed almost negative whereas the sheath potential varied between negative and positive strong dependent on the parameter α which was used to make a difference between an anode conducting electricity and a cool wall isolated. For determining the sheath potential, a formula was established, which took account of the electron temperature, the electron flux and the ion flux at the free-fall edge as well as the parameter α.

1. Introduction

In spite of extensive efforts in the arc physics[1-8], the understanding of the arc behavior still remains incomplete. Especially, there is still a severe lack of basic understanding of the electrode regions of high-intensity arcs and of the associated electrode phenomena. The proximity to the electrode gives rise to extremely steep gradients of the plasma properties

Transactions of JWRI is published by Joining and Welding Research Institute of Osaka University, Ibaraki, Osaka567, Japan.

which render the experimentation even more difficult in this generally hostile environment. Achieving an effective utilization and exploitation of high-intensity arcs requires a through understanding of the plasma properties and its physical processes in the proximity of the anode surface.

The paper is concerned with the anode region of high-intensity arcs, operated in argon atmosphere with plane, water-cooled Cu anodes. The anode region is generally defined as the part of the arc discharge which contains the surface of the anode, the sheath in front of the anode and the boundary layer which makes the connection to the arc column.

Although there has been some research of the anode region of electric arcs over the past years, a consistent theory is still lacking which would, for example, predict the sign and the magnitude of the anode fall in high-intensity arcs. According to the analysis by Nemchinskii and Peretts[9], the electric field strength in the anode boundary layer should be less than that in the adjacent arc column, but the anode fall should still be positive for high-intensity arcs. Bose[10] presented a one-dimensional analysis of the wall region for an argon plasma. The electric current may flow into or from the wall in the normal direction (wall as anode or cathode). He found that the anode potential is slightly negative. Dinulescu and Pfender[11], and also Morrow and Lowke[12] carried out an analysis of the anode boundary layer, which predicts negative anode falls. The former results show that the electric field, starting from a small positive value at the arc column side, turns negative inside the boundary layer and assumes large negative value in the vicinity of the anode. However, they admitted in their paper that there is a major difference in the choice of the boundary condition for solving the conservation equations for the anode boundary layer between the experimental results by their group and their own work. They selected much steeper temperature gradients of the plasma species as boundary conditions and assumed the heavy particle temperature decreases from the value in the plasma to 400 K which is the temperature of the anode surface. Although the water-cooled anode temperature is lower, and electron and heavy particle temperatures separate in the anode boundary layer, it is justified in questioning whether or not the heavy particle temperature is equal to that of the anode surface, because determining the temperature of ions close to the anode is a problem that still remains unsolved[13-14]. Furthermore, it is not clear that a difference between an anode surface which conducts electricity and a cool wall which is isolated (no net current flow). In their analysis, the equation determining the potential drop across the sheath gives a very large negative value (negative anode fall) for the current density range of practical interest.

Our recent experiments of gas-tungsten-arcs show the positive anode fall in lower current and negative one in rather high current very clearly, which is described in following section. There is no unified theory to explain these phenomena, yet.

In this paper, an approach to understand systematically the dominating process in the anode region is attempted.

2. Experiments

Experimental procedures are described in the previous paper[15], therefore, some of results are shown here.

Figure 1 shows the temperature profiles measured in free-burning argon arcs at the arc current of (a) 50 A and (b) 150 A. The each temperature close to the cathode was 13000 K for 50 A and 16000 K for 150 A. Both temperatures decrease with distance from the arc axis and the cathode.

Figure 2 shows the electron and heavy particle temperature distributions in front of the anode at the arc current of 50 A and 150 A. The heavy particle temperature and electron temperature were obtained from the laser scattering measurements and Langmuir probe measurements, respectively. In the case of 50 A, electron temperature immediately increases with approaching the anode in arc axis, but heavy particle temperature decrease. This suggests that the anode boundary layer under this condition remarkably deviates from LTE. On the other hand, in the case of 150 A, electron temperature approximately corresponds with heavy particle temperature at the degree of about 12000 K. This suggests that the boundary layer under this condition preserves the similar state of LTE.

Figure 3 shows the space potential distributions in front of the anode under the

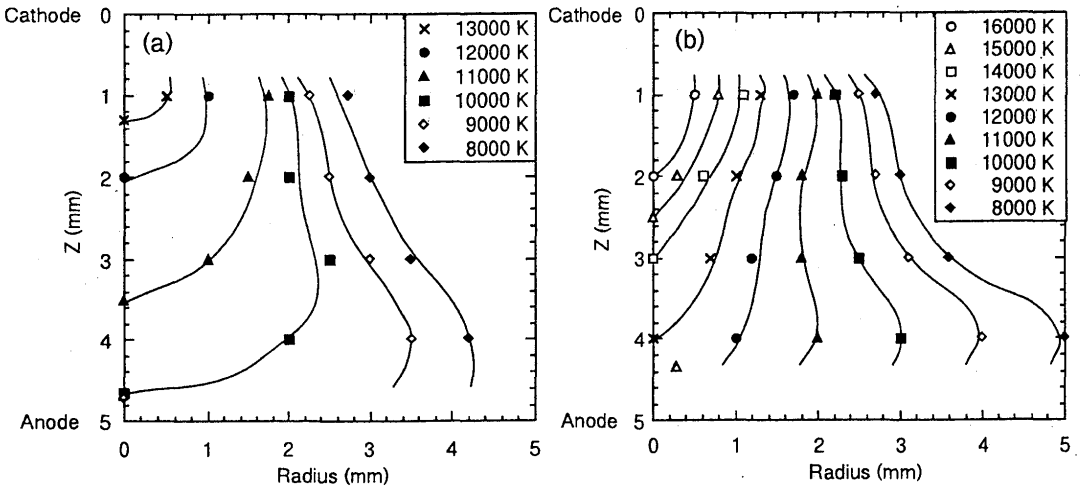

Fig. 1 Temperature profiles under the conditions of (a) 50 A and (b) 150 A.

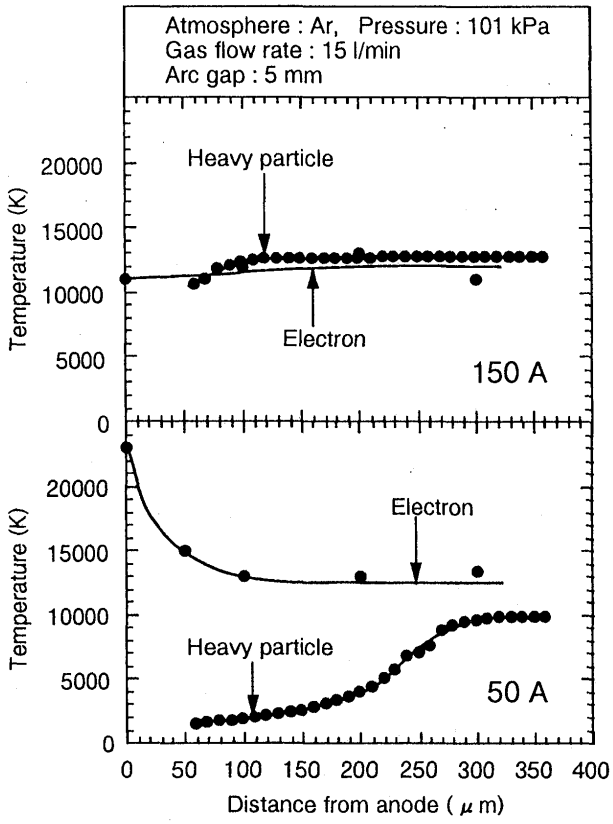

Fig. 2 Electron and heavy particle temperature distributions in front of anode.

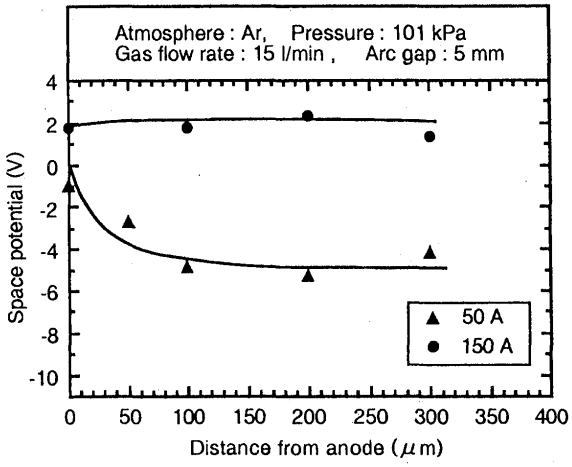

Fig. 3 Space potential distributions in front of anode.

same conditions in Fig. 2. Langmuir probe measurements indicate that the anode fall for 50 A is positive because of decrease in space potential with distance from the anode, but for 150 A seems to be negative because of higher space potential than the anode (= 0 V).

From these results, we can presume the thermal state of the anode boundary layer in free-burning argon arcs, as follows.

In the case of low arc current, such as 50 A, it will provide insufficient thermal ionization due to the lower heavy particle temperature. Therefore it should be necessary the collisional ionization of argon which is caused by electrons. And it will be resulted in the positive anode fall.

In the case of high arc current, such as 150 A, the thermal ionization sustains the arc discharge stably. This means no need of the collisional ionization. Thus, the positive anode fall should not be caused and electrons are not accelerated directionally in the electric field, resulting in the boundary layer preserves the similar state of LTE.

From above discussions, it may be deduced that the thermal state of the anode boundary layer is governed by heavy particle

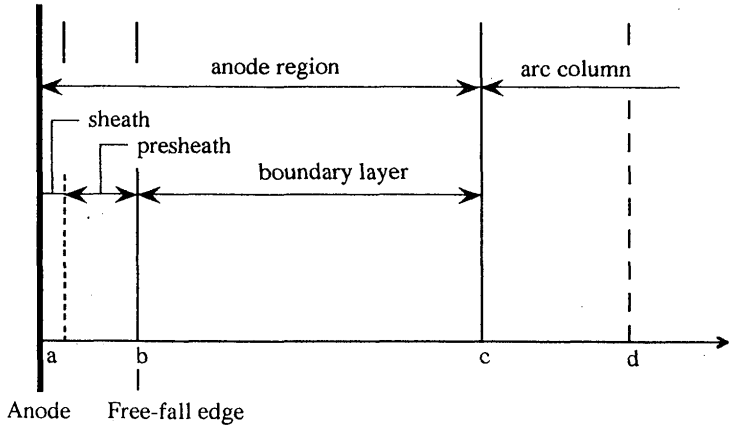

Fig. 4 Schematic sketch of the computational domain.

temperature close to the anode surface and the heavy particle temperature should be influenced decisively by the arc current density.

3. Modeling of Anode Boundary Layer

As shown in Fig. 4, the anode region is divided into three subzones; the anode boundary layer, the presheath and the sheath. In the boundary layer, the presence of the relatively cold anode is felt. The boundary layer is characterized by steep gradients of temperature and particle densities. The boundary layer thickness is in the order of 0.1 mm which is much larger than the particle mean-free-path length. The main feature of the boundary layer is the ionized gas and may be treated as a continuum and as a plasma. Very close to the anode (in the order of one electron mean-free-path), the usual continuum approach is no longer valid. The ionized gas in the presheath and in the sheath may not be treated as a continuum because the total thickness of the presheath and the sheath is equal to one electron mean-free-path. In the presheath, the neutrality of the plasma is maintained. In the Debye sheath, the neutrality is broken and sharp potential drop occurs. The sheath is formed immediately in front of the anode accommodating the transition from electrical conduction in the plasma to metallic conduction in the anode. The thickness of the sheath is in the order of the Debye length.

3.1 Governing equations

Due to its small thickness, the anode region may be treated as a one-dimensional region. For the purpose of solving the conservation equations, the plasma parameters are assumed to vary only in the direction perpendicular to the anode surface. In the boundary layer, the continuum approach and the condition of charge neutrality are valid. Since the electron temperature T_e may be higher than the heavy particle (atoms and ions) temperature T_i, electrons and heavy particles are regarded as two separate fluids coexisting in the plasma.

In a three-component system (electrons, atoms and ions), the electron flux may be written as[16]

$$\vec{\Gamma}_e = n_e \vec{U}_e = -\mu_e n_e \vec{E} - \frac{\mu_e k_B T_e}{e} \nabla n_e - \frac{\mu_e k_B n_e}{e} \nabla T_e \quad (1)$$

where n_e is the electron number density, $\vec{U}_e$ is the electron drift velocity, μ_e is the electron mobility, $\vec{E}$ is the electric field strength, k_B is the Bolzmann constant, and e is the elementary charge. The electron flux is driven by the potential gradient ($\vec{E} = -\nabla\phi$), the electron density gradient and the electron temperature gradient.

The ion flux may be expressed by

$$\vec{\Gamma}_i = n_i \vec{U}_i = \mu_i n_e \vec{E} - \frac{\mu_i k_B T_h}{e} \nabla n_e - \frac{\mu_i k_B n_e}{e} \nabla T_h \quad (2)$$

where n_i is the ion number density, $\vec{U}_i$ is the ion drift velocity, and μ_i is the ion mobility. The condition of charge neutrality is valid in the

boundary layer, thus there is the relation $n_e \approx n_i$. The forces driving the ion flux are the potential gradient, the ion density gradient and the ion temperature gradient.

In a steady state without macroscopic mass flow, the particle conservation equation of the electrons becomes

$$\nabla \cdot \vec{\Gamma}_e = \dot{n}_e \tag{3}$$

where $\dot{n}_e$ is the net electron production rate. Under the same conditions the particle conservation equation for the ions is

$$\nabla \cdot \vec{\Gamma}_i = \dot{n}_e \tag{4}$$

Since electron and ion production occurs in pairs, the net ion production rate equals to that of the electrons.

In the plasma, the net electron production rate is the difference between the ionization rate by electron impact and the three-body recombination rate. In terms of the recombination coefficient γ and species composition, the net electron production rate is given by

$$\dot{n}_e = \gamma n_a \left[\left(\frac{n_e^2}{n_a} \right)_{equil} - \frac{n_e^2}{n_a} \right] \tag{5}$$

where $\left(\frac{n_e^2}{n_a} \right)_{equil}$ is the function of T_e given by Saha equation

$$\left(\frac{n_e^2}{n_a} \right)_{equil} = \frac{2Z_i}{Z} \left(\frac{2\pi m_e k_B T_e}{h^2} \right)^{3/2} exp\left(-\frac{\varepsilon_i}{k_B T_e} \right) \tag{6}$$

where Z_i is the partition function of ion, Z is the partition function of neutral atom, m_e is the mass of electron, h is Plank's constant, n_a is the number density of neutral atoms, and ε_i is the ionization potential. The number density n_a is related to the pressure p by the expression

$$n_a = \frac{p}{k_B T_h} - n_e \left(1 + \frac{T_e}{T_h} \right) \tag{7}$$

The current density is given by

$$\vec{J} = \vec{J}_e + \vec{J}_i \tag{8}$$

where $\vec{J}_e$ and $\vec{J}_i$ represent the electron and the ion contribution, respectively. According to Eqs. (1) and (2), the current density may be expressed as

$$\vec{J}_e = -e\vec{\Gamma}_e, \quad \vec{J}_i = e\vec{\Gamma}_i \tag{9}$$

Based on Eqs. (3) and (4), there is the following relation

$$\nabla \cdot \left(\vec{\Gamma}_e - \vec{\Gamma}_i \right) = 0, \quad \vec{\Gamma}_e - \vec{\Gamma}_i = \text{constant} \tag{10}$$

Thus, in the boundary layer

$$\vec{J} = \vec{J}_e + \vec{J}_i = e\left(\vec{\Gamma}_i - \vec{\Gamma}_e \right) = \text{constant} \tag{11}$$

In a steady state situation without macroscopic mass flow, the energy conservation equation of the electrons may be expressed

$$-\nabla \cdot \left(k_e \nabla T_e \right) + \left(\frac{5}{2} k_B T_e + \frac{e\phi_d}{k_B \sigma} \right) \frac{k_B T_e}{e} J + JE = \left(\frac{5}{2} k_B T_e + \varepsilon_i \right) \dot{n}_e + \frac{3m_e}{m_i} k_B \left(T_e - T_h \right) n_e \bar{\nu}_{ei} \tag{12}$$

where k_e is the electron thermal conductivity, ϕ_d is the thermal diffusion coefficient of the electrons, σ is the electrical conductivity, m_i is the mass of ion, and $\bar{\nu}_{ei}$ is the average collision frequency between electrons and ions. The terms on the left-hand side of Eq. (12) contain several energy input in the sequence, heat transfer by the pure conduction, the transport of enthalpy due to the random thermal energy of electrons and the Thomson effect, and the internal energy dissipation due to Joule heating. The first term on the right-hand side of Eq. (12) represents the energy used for the production of electrons by ionization, while the second term represents the energy losses by elastic collisions between electrons and heavy particles. Here only collisions between electrons and ions have been taken into consideration since in the anode boundary layer the collision frequency between electrons and ions is much larger than that between electrons and atoms[11].

For heavy particles, the Joule heating term due to the ion current may be neglected. The energy equation of heavy particles becomes

$$-\nabla\cdot(k_h\nabla T_h)+\frac{3m_e}{m_i}k_B(T_e-T_h)n_e\bar{\nu}_{ei}=0 \qquad (13)$$

where k_h is the thermal conductivity of heavy particles.

The main unknowns in the set of equations are n_e, T_e, T_h and E. With these key variables all other quantities of interest can be computed. There are also four main differential equations, i.e. , Eqs. (3), (4), (12) and (13). The other equations are auxiliary relations.

3.2 Boundary Conditions

In order to solve the system of equations, appropriate boundary conditions must be specified. Because the thickness of the anode boundary layer L_a is an additional unknown, the boundary conditions can not be specified at the interface between the arc column and the anode boundary layer as there of Dinulescu and Pfender. In this study, the boundary conditions are specified at a place lying in the arc column and taken from the solutions of the arc plasma region. The distance from this place to the anode surface is a little bigger than L_a. The differential equations are solved starting from this place and then entering the anode boundary layer soon.

As shown in Fig. 4, at $x = x_d$; (1) the heavy particle temperature and electron temperature are identical, $T_e = T_h = (T)_{x_d}$; (2) the temperature gradients of heavy particle and electron are identical, $dT_e/dx = dT_h/dx = (dT/dx)_{x_d}$; (3) the electron number density, $n_e = (n_e)_{x_d}$; (4) the gradient of electron number density, $dn_e/dx = (dn_e/dx)_{x_d}$; (5) the current density, $J = (J)_{x_d}$; and (6) the electric field strength, $E = (E)_{x_d}$. Among these six parameters, electron number density and its gradient are both calculated from the Saha equation at $(T)_{x_d}$ and from $(dT/dx)_{x_d}$, while others are determined by the model of arc plasma region[18].

Very close to the anode (in the order of one electron mean-free-path), the usual continuum approach is no longer valid. Thus, the calculation about the anode boundary layer should be stopped at the free-fall edge (point b in Fig. 4), because $x_b = \lambda_e$. An additional boundary condition at the free-fall edge should be specified since the thickness of the anode boundary layer L_a is unknown. The ion temperature in the vicinity of anode surface is still a problem for further study[13-14]. Thus, an adjustable parameter is defined as

$$\theta = \frac{T_{hb}}{T_a} \qquad (14)$$

where T_{hb} is the heavy particle temperature at the free-fall edge, and T_a is the anode surface temperature.

3.3 Solution Methods

The set of conservation equations, i.e., Eqs. (3), (4), (12) and (13), represents four second-order differential equations including highly nonlinear, nonequilibrium thermodynamic and transport properties. By applying the Runge-Kutta procedure, these differential equations are solved starting from boundary conditions and proceeding step by step toward the anode. The values of key variables n_e, T_e, T_h and E are determined in the boundary layer. For each step, the nonequilibrium composition at that particular location is determined first and then the thermodynamic and transport properties are calculated using the methods described in Ref. 19. This procedure continues until the supplementary condition $T_{hb} = \theta T_a$ may be recovered and the variation of the electron number density over one electron mean-free-path reaches the same order of magnitude as the electron number density itself. At this point, the continuum approach is no longer valid. The thickness of the anode boundary layer is defined as the distance from this point to the location where the difference $T_e - T_h$ becomes less than 10% of the electron temperature T_e. The procedure allows the determination of the boundary layer thickness in addition to the local values of plasma properties.

4. Sheath Potential

The anode fall is the potential drop in the anode region[10]. After solving the main

differential equations, the potential difference in the boundary layer, i.e. , $\phi_{\lambda_e} - \phi_{L_a}$ can be calculated. The potential change from the anode surface to the free-fall edge, i.e. , $\phi_a - \phi_{\lambda_e}$, may be called the sheath potential which consists of the presheath and Debye sheath[14]. The sheath potential may be determined by the following approach;

First, let us consider a situation in which a plasma borders a wall. Charged particle density gradients are particularly steep close to plasma-confining walls. The gradients of electron and ion density in the vicinity of the wall drive electron and ion fluxes toward the wall, but the electron flux initially exceeds the ion flux because of the higher electron mobility. Since the wall is assumed to be isolated (no net current flow), it will acquire a negative potential, producing an electric field that points toward the wall. This field subsequently balances electron and ion fluxes (electrons are retarded and ions are accelerated), thus in a steady-state situation electrons and ions reach the wall at the same rate and recombine on impact with the wall. This process is known as *ambipolar diffusion*. In this case the wall serves as the third partner for three-body recombination. A net positive space charge is formed in the sheath overlying the wall surface, because electrons are repelled and positive ions are attracted by the wall.

The electron flux Γ_e, the ion flux Γ_i, and the electron temperature T_e at the free-fall edge ($x_b = \lambda_e$) can be determined from the calculations of the anode boundary layer described above. To determine the sheath potential $\phi_a - \phi_{\lambda_e}$, we need to calculate first the electron flux striking the wall. On the average, electrons striking the wall experience their last collision in a distance approximately one mean-free-path λ_e away from the wall. Only those electrons with sufficient energy to overcome the potential barrier will reach the wall[16]. The electron flux striking the wall is given by the expression

$$\Gamma_{ea} = \Gamma_{eb} exp\left[\frac{e\left(\phi_a - \phi_{\lambda_e}\right)}{k_B T_{eb}}\right] \qquad (15)$$

Since the ions are not impeded by the sheath potential, the ion flux is conserved across the region[13]

$$\Gamma_{ia} = \Gamma_{ib} \qquad (16)$$

Because electrons and ions reach the wall at the same rate, the following relation exists[16];

$$\Gamma_{ea} = \Gamma_{ia} \qquad (17)$$

Then, let us consider the situation in which a plasma borders an anode. The anode conducts electricity. Some electrons enter the lattice of the anode and release energy proportional to the anode work function[1, 17]. An adjustable parameter α is defined to describe the percentage of electrons entering the lattice of anode. Therefore, at the anode surface, there is the following relation

$$(1-\alpha)\Gamma_{ea} = \Gamma_{ia} \qquad (18)$$

The sheath potential is obtained from this condition

$$(1-\alpha)\Gamma_{eb} exp\left[\frac{e\left(\phi_a - \phi_{\lambda_e}\right)}{k_B T_{eb}}\right] = \Gamma_{ib} \qquad (19)$$

After manipulating, this condition yields

$$\phi_a - \phi_{\lambda_e} = \frac{k_B T_{eb}}{e} ln\left[\frac{\Gamma_{ib}}{(1-\alpha)\Gamma_{eb}}\right] \qquad (20)$$

Since T_{eb}, Γ_{eb} and Γ_{ib} have been computed from the analysis of anode boundary layer, the sheath potential $\phi_a - \phi_{\lambda_e}$ can be easily calculated. If α is equal to zero, it is the case of a isolated wall. Under this condition, the sheath potential is always negative because Γ_{eb} is much larger than Γ_{ib} . With increasing the value of α , the absolute value of the sheath potential decreases. When α increases to a certain value, the sheath potential turns positive.

5. Results and Discussions

As mentioned in section 3.2, based on the model of fluid flow and heat transfer in an argon arc plasma[18], values of T_e, T_h, dT_e/dx, dT_h/dx, J and E at a location lying in the arc

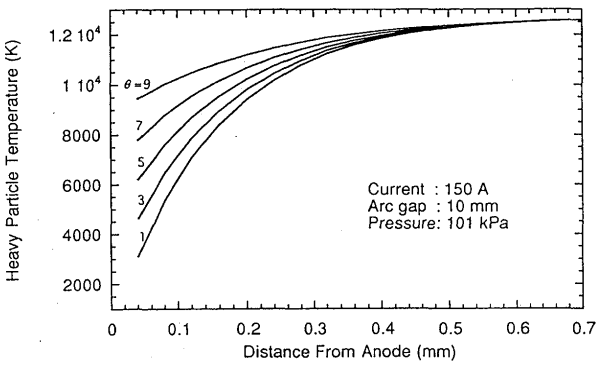

Fig. 5 Distribution of T_h in the anode boundary layer.

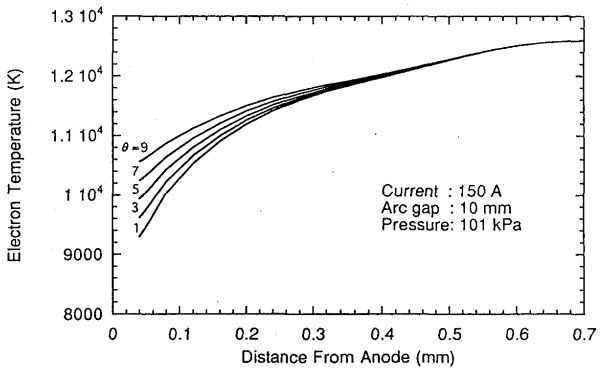

Fig. 6 Distribution of T_e in the anode boundary layer.

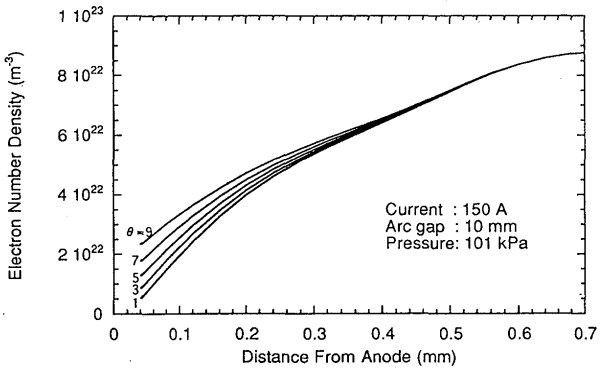

Fig. 7 Distribution of n_e in the anode boundary layer.

column can be determined. Values of n_e and dn_e/dx can be calculated from the Saha equation at T_e and from dT_e/dx. These values are used as the boundary conditions. For a free-burning argon arc at 150 A and 1 atmosphere pressure, the corresponding boundary conditions are specified as follows:

at $x = x_d$:

$$T_e = T_h = 1.26 \times 10^4 K$$

$$\frac{dT_e}{dx} = \frac{dT_h}{dx} = 4.5 \times 10^5 K/m$$

$$n_e = 8.82 \times 10^{23}\ 1/m^3$$

$$\frac{dn_e}{dx} = 2.38 \times 10^{25}\ 1/m^4$$

$$J = 3.2 \times 10^6\ A/m^2$$

$$E = 5.2 \times 10^2\ V/m$$

Figures 5 and **6** show the temperature distributions for heavy particles and electrons, respectively. It can be seen that the value of parameter θ, i.e., the ratio of the heavy particle temperature at the free-fall edge to the anode surface temperature, has a marked effect on the temperature distributions in the boundary layer. The lower the heavy particle temperature at the free-fall edge, the steeper the temperature gradients for both electrons and heavy particles in the boundary layer. **Figure 7** shows the distribution of electron number density at different values of θ. It has a same trend as the temperature distribution because of the strong dependence of electron number density on electron temperature.

Shown in **Figs. 8** and **9** are the electric field strength and the electrical potential in the boundary layer. The electric field strength at the free-fall edge changes from -0.8×10^4 V/m to -5.2×10^4 V/m when θ varies from 9 to 1. This fact means that steeper gradients of temperature and electron number density cause an increase of the electric field strength resulted from diffusion in the boundary layer. Correspondingly, the electrical potential at the free-fall edge decreases when θ varies from 9 to 1.

Table 1 demonstrates the influence of the parameter θ on plasma scale lengths and potential drop in the boundary layer. The boundary layer thickness L_a, the electron mean-free-path λ_e, the Debye length λ_D, and the potential drop $\phi_{\lambda_e} - \phi_{L_a}$ in the boundary layer are all computed from the solution of the governing equations of the anode boundary layer. The results indicate that the boundary layer thickness decreases as the value of θ increases. A bigger value of θ results in smaller temperature gradients for electrons and ions, which make the deviation between the electron temperature and the heavy particle temperature emerge at a point nearer the free-fall edge so that the boundary layer thickness decreases. The computed results show that the boundary layer

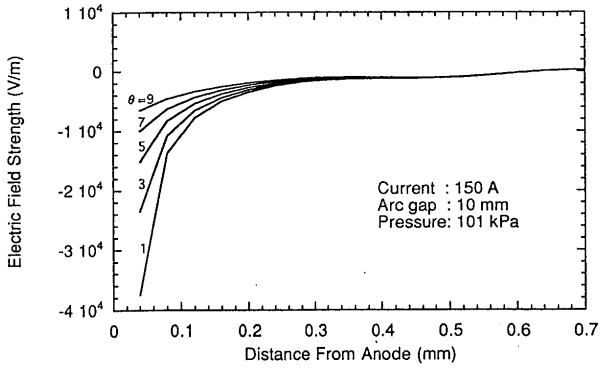

Fig. 8 Electric field distribution in the anode boundary layer.

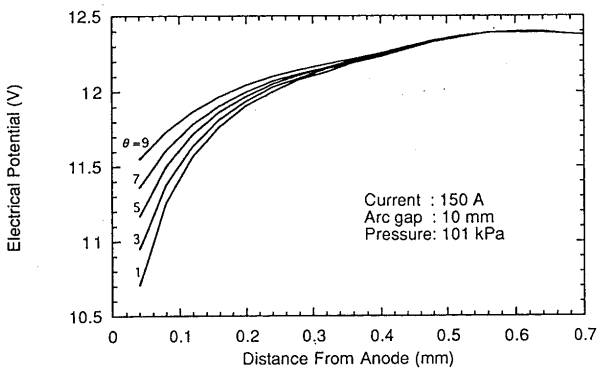

Fig. 9 Electrical potential distribution in the anode boundary layer.

Table 1 The influence of the ratio $\theta = T_{hb}/T_a$ on plasma scale length and potential drop in the anode boundary layer (current : 150 A, arc gap : 10mm, pressure : 101 kPa).

θ	L_a (mm)	λ_e ($\times 10^{-2}$ mm)	λ_D ($\times 10^{-5}$ mm)	$\phi_{\lambda_e} - \phi_{L_a}$ (V)
1	0.240	0.290	9.208	-1.395
3	0.240	0.436	7.343	-1.183
5	0.200	0.590	6.109	-0.894
7	0.160	0.754	5.262	-0.622
9	0.040	0.934	4.642	-0.061

thickness is two orders of magnitude larger than the electron mean-free-path which, in turn, two orders of magnitude larger than the Debye length. With increasing of the value of θ, the potential drop in the boundary layer varies from a distinctly negative to a nearly zero.

It is quite evident that the parameter θ has great influences on the local plasma properties in the boundary layer and the boundary layer thickness. With the same boundary conditions at the arc column side, the values of heavy particle temperature at the free-fall edge play an important role in determining the key variables in the boundary layer. Up to now, the heavy particle temperature very close to the anode surface is still unclear. Some analyses are restricted to the case of cold ions[13]. Some researchers considered the finite temperature of the ions[14]. But there are no concrete and definite values of the ion temperature in the vicinity of the anode. Therefore, it is necessary to make an estimate of the heavy particle temperature at the free-fall edge.

The calculated results shown hereinafter are under the condition of $\theta=5$. **Figure 10** shows that the electron temperature and the heavy particle temperature are identical at the arc column side. They deviate increasingly from each other towards the anode. The heavy particle temperature drops from 12600 K in the arc column to 5000 K at the free-fall edge while the electron temperature decreases from 12600 K to 9200 K. The electron temperature maintains sufficiently high value over the entire thickness of the anode boundary layer to ensure the required electrical conductivity for the passage of the electric current. The electron density derived from the conservation equations and the equilibrium electron density determined from the Saha equation are plotted in **Fig. 11**. In the proximity of the anode surface, the difference between the actual value and the Saha value is quite pronounced. This is due to the fast diffusion of the electrons toward the anode.

The electron flux and its components are shown in **Fig. 12**. The curve denoted by Γ_e^E represents the flux component driven by the electric field, expressed by the first term on the

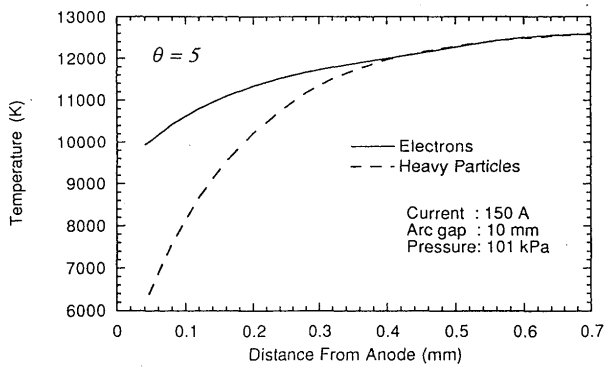

Fig. 10 Species temperature distribution in the anode boundary layer.

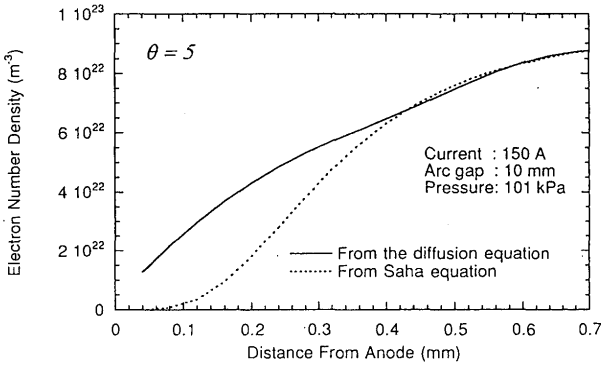

Fig. 11 Electron number density distribution in the anode boundary layer.

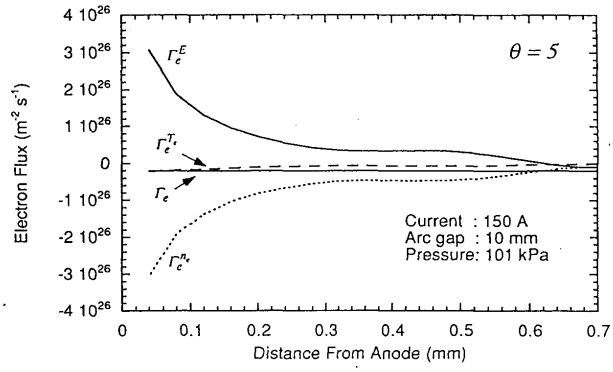

Fig. 12 Distribution of electron flux and its components in the anode boundary layer.

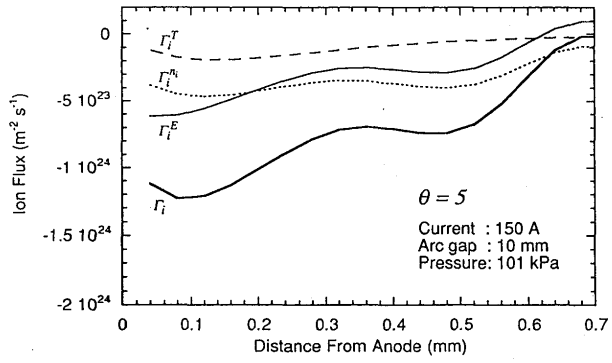

Fig. 13 Distribution of ion flux and its components in the anode boundary layer.

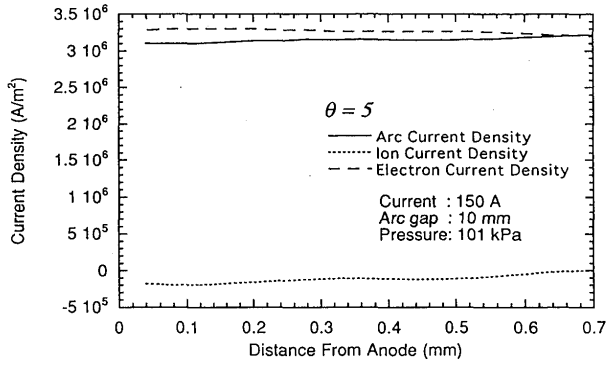

Fig. 14 Current density in the anode boundary layer.

right-hand side of Eq. (1). The second and the third term of this equation are represented by the curves $\Gamma_e^{n_e}$ and $\Gamma_e^{T_e}$, respectively. The temperature and electron density gradients push the electrons toward the anode. The electric field drives the electrons toward the anode first. But as approaching the anode slightly, it drives the electrons away from the anode.

Although the electric field strength is very high near the free-fall edge, this opposing force is overbalanced by the rapid increasing gradients of the electron density and temperature close to the free-fall edge which keep the electrons flowing toward the anode. It is obvious that the electron density gradient plays a more important role in driving the electron flux. **Figure 13** shows the ion flux and its components. The electric field drives the ions away from the anode first. But as approaching the anode slightly, it turns to push the ions toward the anode. The important driving forces for the ion flux are the ion temperature gradient and ion density gradient.

The current density and its components are plotted in **Fig. 14**. Far away from the anode, the ion current is positive (directed away from the anode). As the ions approach the anode, the ion current becomes negative because of the effect described in Fig. 13. The electron current density is much larger than the ion current and approximately corresponds with total current which is the arc current density. It is evident that the dominant component of the current is the electron current and the ion current is negligibly small.

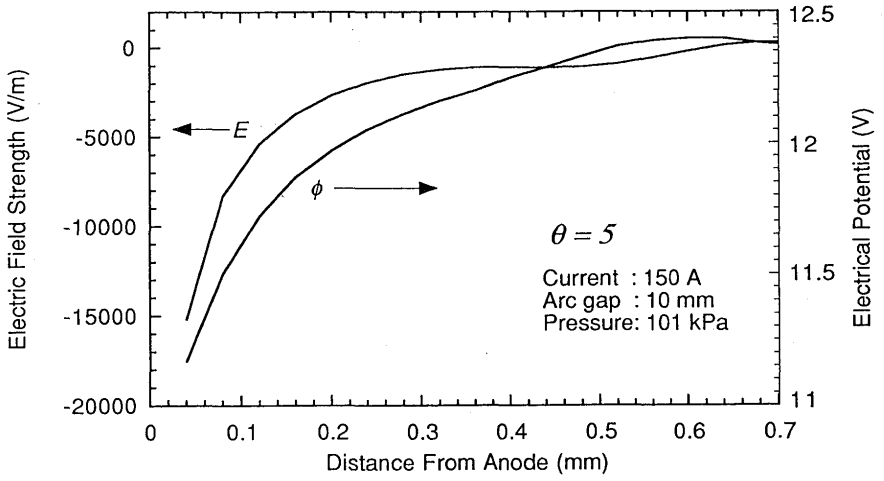

Fig. 15 Electric field strength and electrical potential in the anode boundary layer.

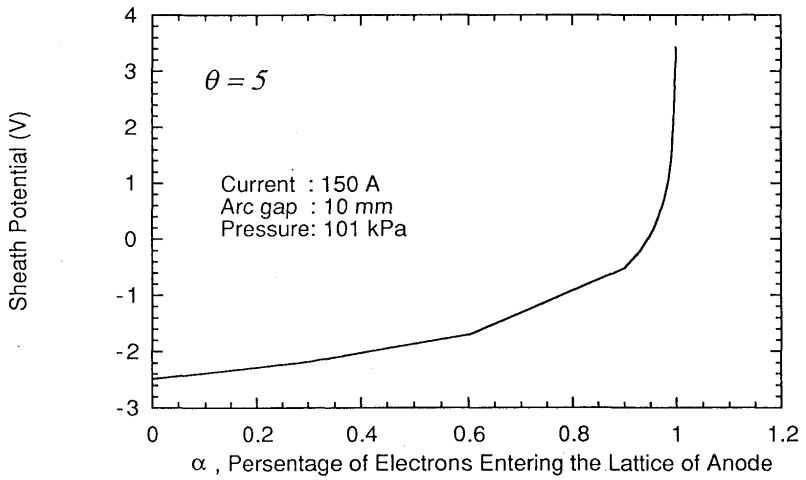

Fig. 16 Sheath potential as a function of parameter α.

Figure 15 shows the distribution of the electric field strength and the electrical potential in the boundary layer. The electric field, starting from a small positive value at the arc column side, decreases inside the boundary layer and turns to negative. As approaching the anode, the electric potential first increases and then falls. The decrease of the potential signifies that the electric field in the boundary layer is opposing the motion of the electrons and accelerating the positive ions. The net potential drop in the whole boundary layer is slightly positive.

Figure 16 demonstrates the relation between the sheath potential and the parameter α. It is quite clear that the percentage of the electrons entering the lattice of anode has a very marked effect on the sheath potential. When α is equal to zero, it is the case of a wall in which the sheath potential is -2.5 V. When α is less than 0.94, the sheath potential is negative. Under this condition, the absolute value of the sheath potential decreases with increasing the value of α. When α is equal to 0.94, the sheath potential becomes zero. For α greater than 0.94, the sheath potential turns positive. The prerequisite for Eq. (20) is that α can not take the value of 1. Otherwise, that equation becomes meaningless. For a case of $\alpha = 0.999$, the sheath potential becomes 3.5 V. These results show that if more electrons enter the lattice of anode, the negative potential across the sheath gets lower because a weaker electric field is required to balance electron and ion fluxes close to the anode. If over 94% of electrons enter the anode, the sheath potential becomes positive because in this case a net negative space charge is formed in the sheath.

Table 2 The sheath potential at different levels of θ and α (current : 150 A, arc gap : 10mm, pressure : 101 kPa, unit : V).

α	$\theta=1$	$\theta=3$	$\theta=5$	$\theta=7$	$\theta=9$
0.000	-2.787	-2.551	-2.488	-2.524	-2.634
0.300	-2.502	-2.256	-2.183	-2.209	-2.309
0.600	-2.053	-1.792	-1.704	-1.715	-1.800
0.900	-0.943	-0.643	-0.517	-0.492	-0.538
0.930	-0.658	-0.348	-0.212	-0.177	-0.214
0.944	-0.479	-0.163	-0.021	0.020	-0.011
0.948	-0.420	-0.101	0.042	0.085	0.057
0.956	-0.286	0.037	0.185	0.233	0.209
0.964	-0.125	0.203	0.357	0.410	0.391
0.968	-0.031	0.301	0.458	0.514	0.498
0.976	0.200	0.539	0.704	0.768	0.760
0.980	0.346	0.690	0.860	0.929	0.926
0.984	0.524	0.875	1.051	1.126	1.129
0.990	0.901	1.265	1.453	1.541	1.557
0.996	1.634	2.024	2.237	2.349	2.391
0.998	2.189	2.599	2.831	2.961	3.022
0.999	2.745	3.173	3.424	3.573	3.652

And also it should be taken notice that positive large value of sheath potential may provide the positive anode fall by over compensating the negative potential over the boundary layer.

Two adjustable parameters θ and α are introduced in this paper. **Table 2** gives the sheath potential at different values of θ and α. It is clear that both parameters are very important and of great influences on the computed results. It should be stressed that these complex problems about the anode region and anode fall are far from being fully solved. A great deal more work will be required to study the mechanism of interactions between the electrons and the anode surface, and determine the exact percentage of the electrons entering the lattice of anode.

6. Conclusions

The conclusions in this paper are summarized as follows.

In experiments;

(1) In the case of a low current region, the anode boundary layer remarkably deviated from LTE because of the higher electron temperature and the lower heavy particle temperature. In this case, anode fall was positive.

(2) In the case of a high current region, the anode boundary layer preserved the similar state of LTE because of correspondence between the electron temperature and the heavy particle temperature. In this case, anode fall was negative.

(3) In this work, the thermal state of the anode boundary layer has strong relation to the heavy particle temperature close to the anode surface.

In modeling;

A model is studied for analyzing the physical behavior of the anode region in a high-intensity, atmospheric pressure free-burning argon arc. The boundary conditions for modeling the anode region are taken from the solutions of gas-tungsten-arc LTE plasma. Based on the results of this study the following conclusions may be drawn;

(4) The ratio of the heavy particle temperature at the free-fall edge to the anode surface temperature has a great influence on the local plasma properties in the boundary layer, the boundary layer thickness and the sheath

potential.

(5) The thickness of the anode boundary layer is found to be approximately 0.20 mm for 150 A arcs at an arc length of 10 mm. It is two orders of magnitude larger than the electron mean-free-path which, in turn, is two orders of magnitude larger than the Debye length.

(6) In the anode boundary layer, the electron flux is mainly driven by the electron density gradient whereas the most important driving force for the ion flux is the ion temperature gradient and ion density gradient.

(7) The potential drop in the anode boundary layer without sheath existing just in front of the anode is negative.

(8) The percentage of the electrons entering the lattice of anode has a very marked effect on the sheath potential. With different values of this percentage, the sheath potential may be negative, zero or positive. It needs further study to determine this percentage and the dominant factors influencing it.

References

1. M.I. Boulos, P. Fauchais and E. Pfender: Thermal Plasmas, vol.1, Plenum Press, New York, NY, 1994, pp.6-43.
2. K.C. Hsu, K. Etemadi and E. Pfender: J. Appl. Phys., 1983, vol.54, pp.1293-1301.
3. O.H. Nestor: J. Appl. Phys , 1962, vol.33, pp.1638-1648.
4. A.E. Guile, M.A. Hilton and I.A. McLelland: J. Phys. D: Appl. Phys., 1975, vol.8, pp.964-970.
5. R.S. Devoto: Phys. Fluids, 1967, vol.10, pp.2105-2112.
6. A.D. Morris and W.C. Gore: Weld. J., 1956, vol.35, pp.137s-144s.
7. C.J. Allum: Weld. Met. Fabr. , 1982, vol.50, pp.124-132.
8. N.A. Sanders and E. Pfender: J. Appl. Phys., 1984, vol.55, pp.714-722.
9. N.A. Nemchinsky and L.N. Peretts: Zh. Tekh. Fiz., 1977, vol.47, pp.1868-1875.
10. T.K. Bose: Plasma Chem. Plasma Proc., 1990, vol.10, pp.189-206.
11. H.A. Dinulescu and E. Pfender: J. Appl. Phys., 1980, vol.51, pp.3149-3157.
12. R. Morrow and J.J. Lowke: J. Phys. D: Appl. Phys., 1993, vol.26, pp.634-642.
13. G.A. Emmert, R.M. Wieland, A.T. Mense and J.N. Davidson: Phys. Fluids, 1980, vol.23, pp.803-812.
14. I. Senda: Phys. Plasmas, 1995, vol.2, pp.6-13.
15. M. Tanaka and M. Ushio: Proceedings of the 3rd Asia-Pacific Conference on Plasma Science & Technology, 1996, Tokyo, Japan, pp.397-401
16. M. Mitchner and C.H. Kruger, Jr. : Partially Ionized Gases, Wiley, New York, NY, 1973, pp.146-155.
17. J. McKelliget and J. Szekely: Metall. Trans, 1986, vol.17A, pp.1139-1148.
18. M. Ushio, C.S. Wu and M. Tanaka: Report 96-949, Welding Arc Physics Committee of Japan Welding Society, 1996.
19. H.A. Dinulescu: Ph.D. thesis, University of Minnesota, 1979.
20. M. Ushio, D. Fan and M. Tanaka: Trans. JWRI, 1993, vol.22, pp.201-207.
21. N.S. Tsai and T.W. Eagar: Metall. Trans. , 1985, vol.16B, pp.841-846.